Peltier Supercooling with Isosceles Current Pulses: Cooling an Object with Internal Heat Generation

Alfred J. Piggott[a,b,*,z] **and Jeffrey S. Allen**[a,*]

[a]*Michigan Technological University, Houghton, Michigan 49931, USA*
[b]*Applied Thermoelectric Solutions LLC, Novi, Michigan 48375, USA*

Applying a current pulse enables a short-term transitory state where the cold junction of a Peltier couple reaches temperatures below that obtainable via maximum temperature delta steady-state current. Short-term cooling applications like on-chip hot spot and pulsed laser sensor cooling have been studied using pulsed cooling. Some studies have proposed applications that utilize consecutive repeating pulses for longer term cooling applications. These studies have found or theorized increased cooling and coefficient of performance (COP). Considering these studies, it is desirable to have a more detailed analysis of how the additional cooling and COP are achieved. The objective herein is to provide a detailed analysis of cooling rate and COP during pulses using a realistically modeled system simulated in SPICE. It was found that cooling rate for long term consecutive pulse cooling applications can be increased over steady-state but COP in most cases is reduced during current pulses. The reasons why this happens are studied in depth.
© The Author(s) 2017. Published by ECS. This is an open access article distributed under the terms of the Creative Commons Attribution 4.0 License (CC BY, http://creativecommons.org/licenses/by/4.0/), which permits unrestricted reuse of the work in any medium, provided the original work is properly cited. [DOI: 10.1149/2.0391712jss]

Manuscript submitted September 5, 2017; revised manuscript received December 4, 2017. Published December 29, 2017. This was Paper 1159 presented at the National Harbor, Maryland Meeting of the Society, October 1–5, 2017.

From portable electronics to large scale systems and power electronics used for transportation, demand for more economical and effective heat removal means is growing.[1]

Peltier devices offer a means of moving heat that has many advantages. Peltier coolers are solid-state heat pumps that convert electric current directly into a temperature difference and heat flux. The devices are reversible, imposing a temperature difference will induce a current flow. The thermoelectric effect is the operating principle utilized.

As a thermal management method, using thermoelectrics has many advantages. Thermoelectrics are solid-state. Having no moving parts increases reliability and allows for no noise or vibration. Heating and cooling can be achieved from the same device at the same time. The heat flow direction can be reversed by reversing the electrical polarity to the device. The electrical current to the device can be controlled very precisely and this allows temperature control within +/− 0.01 °C.[2] With thermoelectrics, below ambient temperatures can be achieved. A coefficient of performance (COP) greater than 1 can be achieved for heating which is not possible for resistive Joule heaters. Thermoelectrics offer high cooling power density and can be designed for very high cooling COP.[3] In addition to high COP, power consumption can be reduced since the devices can be used for site specific or zonal thermal management rather than cooling an entire enclosure. Thermoelectrics use no harmful refrigerants. The devices will operate in an orientation.

Due to the many advantages,[4] thermoelectrics are used for a wide range of diverse applications. More recent studies and applications include using thermoelectric cooling to increase the efficiency of photovoltaic systems,[5] solving thermal management challenges with cooling integration into Silicon Photonic Systems,[6] high COP cooling of aerospace electronics,[3] integration of thermoelectric cooling with phase change materials (PCM) for energy efficient building applications,[7] atmospheric water generation for arid climates,[8] highly efficient water distillation,[9] improved thermal comfort automotive zonal HVAC[10,11] and for hybrid and electric vehicle battery thermal management.[12–18]

Some of many commercialized applications include CPU cooling,[19] kiosk cooling,[20] heated and cooled vehicle seats,[18,21] small refrigerators,[22] mattresses, seats, office chairs,[21] vehicular cup holders and mini refrigerators.[23]

The cooling performance of thermoelectric devices is dependent on the semiconductor materials used, the number of thermocouples, the geometry of the thermoelements that make up the couples, the electrical operating condition of the device and the external heat loading and temperatures.[24]

A growing area of research[12,24–55] is that of transient electrical current operation of thermoelectric devices. When a current pulse is applied to a device operating at steady-state current, a temporary lower temperature can be achieved at the cold junction of the couple or module than can be achieved with the optimum steady state current operation. This is illustrated in Figure 1. This temporary state of lower temperature is called supercooling. Conversely supercooling (transient advantage) is followed by a period of superheating (transient penalty) for which the cold junction temperatures rise above the steady state value. The areas of supercooling and superheating are encompassed in shaded areas of Figure 1. It has been found that the current pulse duration and height can be optimized for maximum transient advantage or to maximize the net cooling which is the difference of transient advantage and transient penalty.[24] Outside of cooling applications, it has been shown that heat pulses can improve the thermal to electric conversion efficiency of thermoelectric generators.[56–61]

Equation 1, sometimes called the "Ideal equation",[62] determines the amount of cooling that can be achieved during steady state operation. The equation holds for transient conditions with the exception that T_c, ΔT and I are time dependent. T_c is the cold side junction temperature of the couple and n is the number of couples in the module. In both cases, α, R and K are temperature dependent.

$$\dot{Q}_c = n\left[\alpha T_c I - \left(\frac{1}{2}\right) I^2 R - K\Delta T\right] \quad [1]$$

This equation is made up of a Peltier, Joule and Fourier term from left to right. α is the Seebeck coefficient of the couple $\alpha = \alpha_p - \alpha_n$ [V/K], T_c is the temperature of the cold junction of each thermoelement, and I is the electric current applied to the couple. R is electrical resistance of the couple in units of ohms. K is the thermal conductance of the couple in [W/K]. ΔT is T_h minus T_c. R is dependent on the semiconductor material electrical resistivity ρ and geometry of the thermoelements. K, the thermal conductance is dependent on the semiconductor thermal conductivity k and geometry of the thermoelements. When $T_h > T_c$ and α is increased while ρ and k decreased, $\dot{Q}_c$ will increase. The same is true for $T_c > T_h$ however $\dot{Q}_c$ decreases as k decreases. The figure of merit, $Z = \alpha^2/\rho k$ is used to characterize thermoelectric semiconductor materials. A higher Z leads to increased $\dot{Q}_c$ when $T_h > T_c$.

Figure 1 shows T_c vs. time when a current pulse is applied. The instant lower temperature achieved followed by a temperature rise and overshoot is due to different time constants of the Peltier cooling

*Electrochemical Society Member.
[z]E-mail: alfred@thermoelectricsolutions.com

Redistribution subject to ECS terms of use (see ecsdl.org/site/terms_use) unless CC License in place (see abstract).

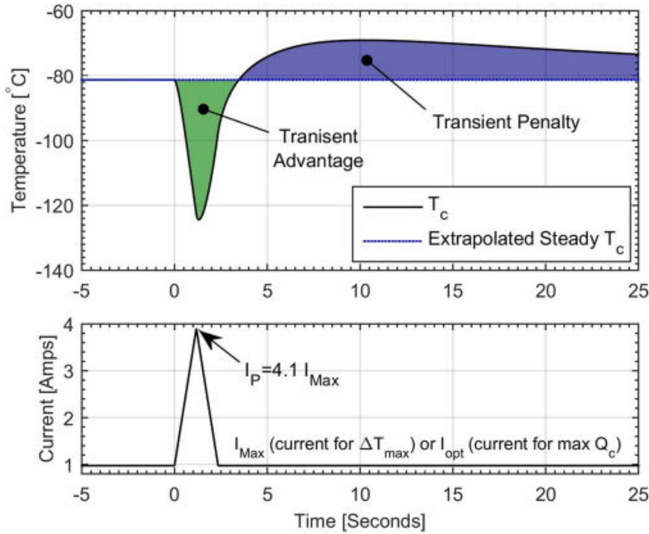

Figure 1. Transient Advantage and Penalty.

and Joule heating terms of Equation 1. Increased Peltier cooling is an instantaneous and interfacial effect that only takes place at the cold junction of each couple. Joule heating takes place instantly throughout the volume of each thermoelement. The volumetric Joule heat has a slower time constant and is delayed from reaching the T_c junction by diffusion throughout the thermoelement.

Equation 2 defines the heat released $\dot{Q}_h$ by the hot side T_h due to Peltier heating.

$$\dot{Q}_h = n\left[\alpha T_h I + \left(\frac{1}{2}\right) I^2 R - K\Delta T\right] \quad [2]$$

The rate of work done by the power input to a thermoelectric device is determined by an energy balance with a boundary around the couple.

$$\dot{W}_n = \dot{Q}_h - \dot{Q}_c \quad [3]$$

Substitution of Equation 1 and Equation 2 into Equation 3 we have

$$\dot{W}_n = n\left[\alpha I(T_h - T_c) + I^2 R\right] \quad [4]$$

The coefficient of performance (COP) is:

$$COP = \frac{\dot{Q}_c}{\dot{W}_n} \quad [5]$$

The coefficient of performance is important because it defines a way to characterize how many watts of thermal power, $\dot{Q}_c$ are moved for every watt of electrical power that is input to the device.

Two values of steady state electric current are the focus of this work. These current values are the values at which the device operates prior to the pulse and after the pulse during pulsed operation. The first value, $I_{\max}$ is the electrical current that sustains the maximum temperature difference between T_h and T_c when T_h is fixed and T_c is insulated. The second, I_{opt} is the electrical current that sustains maximum $\dot{Q}_c$ when $T_h - T_c = 0$. $I_{\max}$[63] and I_{opt}[64] are characterized as follows:

$$I_{\max} = \frac{\alpha}{R}\left[\left(T_h + \frac{1}{Z}\right)^2 - T_h^2\right]^{1/2} - \frac{1}{Z} \quad [6]$$

$$I_{\text{opt}} = \frac{\alpha T_h}{R} \quad [7]$$

The Seebeck coefficient of the couple is $\alpha = \alpha_p - \alpha_n$ [V/K]. R is the electrical resistance of the couple.

For the work herein, isosceles triangle shaped pulses are utilized. For any pulse shape,[47] a normalized method[36] to characterize the pulse magnitude relative to steady state current is defined by Equation 8 and Equation 9. For this work, a pulse magnitude of 1.418 and duration of 10 seconds was used for figures with constant pulse-height or duration. This combination was optimized for net transient advantage for pulses starting from I_{max}[24] using the same thermoelements used herein. For comparison purpose, the same pulse magnitude and duration was used for pulses starting from I_{opt} however this pulse was not optimized for net transient advantage because net transient advantage is not possible starting pulses from I_{opt}.[24]

$$P = \frac{I_p}{I_{max}} \quad [8]$$

$$P = \frac{I_p}{I_{opt}} \quad [9]$$

The time constant for thermal decay[36] from peak transient penalty back to steady state temperature is given by Equation 10.

$$\tau = \frac{4l^2}{\pi^2 a} \quad [10]$$

Here l is the length of the thermoelement and a is the thermal diffusivity of the thermoelement.

SPICE (Simulation Program with Integrated Circuit Emphasis) was developed in the 1970's for solving integrated circuit problems. SPICE has been used to model transient thermoelectrics.[24,38,64–66] The electrical components in the SPICE model are used to replicate the thermal physics with use of thermal analogies to specify the value of the electrical components.

A SPICE model was used for the work herein due its speed, accuracy and it was a natural fit with the previously developed SPICE model.[24] The thermoelectric module model used herein has been validated against other models as well as experimental data with good agreement.[24]

Many studies[12,24–54] have looked at pulse cooling from the standpoint of a single free standing couple with a very small or no attached object to be cooled. Furthermore, these studies were from a cold side temperature perspective only.

Due to the short burst of cooling provided with a pulse that is greater than maximum possible at steady-state, applications have been proposed that use pulse cooling in a continuous manner by utilizing repeated pulses.[55,67] Furthermore, some have surmised[68] that pulse cooling could be used to increase COP to greater than that of steady-state cooling if the right pulse shape is applied.

For each of these proposed applications or studies, it would be useful for the reader to have additional data to understand the physics of how cooling or COP was or could be increased. In one example, a free standing couple was built for which the cold side could be mechanically disconnected[67] after pulsed Peltier cooling and before the time delayed Joule heat (transient penalty) reached the cold side. Then, the cold side is reconnected after the Joule heat dissipates through T_h. With this study, cold side temperature reduction was related to ZT enhancement however it was not clear if the temperature reduction was for the first pulse or for one of the repeated pulses. It would be beneficial to the reader to see temperature, power consumption, $\dot{Q}_c$ and COP vs. time to understand how the system works.

Another example,[55] utilized current pulses and at the same time pulsed the heat transfer coefficient on the hot side of the device. A higher COP was achieved with pulsing then with steady state. However, again there was no transient data for temperature, $\dot{Q}_c$, Power consumption, COP or baseline COP data shown prior to the pulse.

Finally it was reasoned that pulse cooling could increase COP[68] however no results were shown to confirm or quantify it.

These previous studies highlight the need to show the pertinent transient data along with a transient steady-state baseline, explain the physics and to do so using a model of a realistic and system. Fulfilling this need as well as looking at how changing various system level

Redistribution subject to ECS terms of use (see ecsdl.org/site/terms_use) unless CC License in place (see abstract).

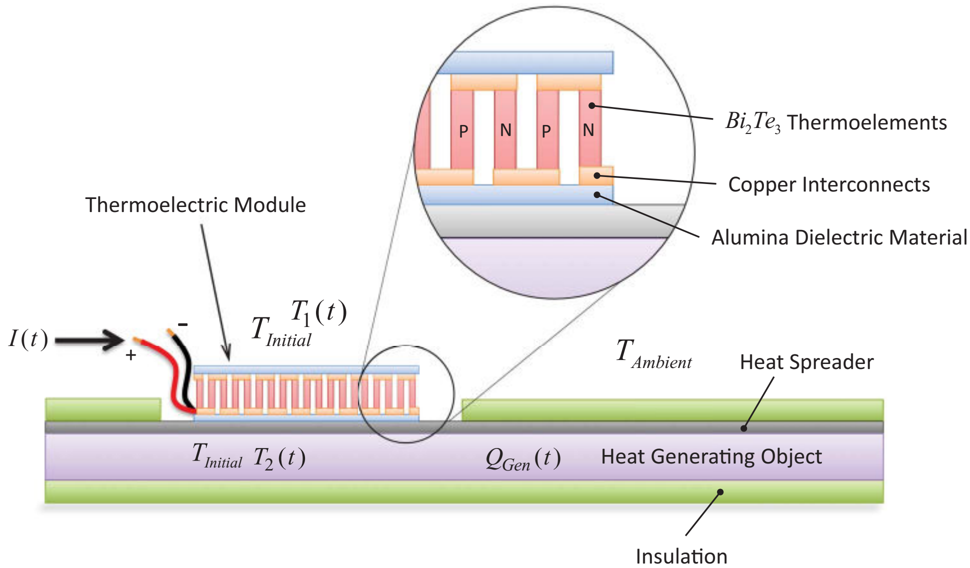

Figure 2. System - Heat Generating Object Cooled by Thermoelectric Module.

variables effect the response of COP and $\dot{Q}_c$ is the objective of the study herein.

To accomplish the objective, an optimized isosceles shaped current pulse with current pulse-height and duration taken from Ref. 24 was applied to a thermoelectric module in thermal contact with a system containing a relatively large heat generating object. The work herein also added interface resistances and internal Joule heat generation within the copper interconnects. This has not been previously studied. These additional details created a realistic application for which pulse cooling could be studied.

Previous studies used pulses starting from only I_{max}. The work herein also used pulses starting from I_{opt} for comparison to see if pulses can deliver more cooling than the maximum that can be achieved in steady state.

The work herein studied the effects of varying the different aspects of the system. These include, internal heat generation of the cooled object and interface resistances between the module and heat spreader and between the heat spreader and cooled object. These studies have not been previously performed.

This research will help focus future work toward achieving the iNEMI road map goal[1] of finding more economical and effective means of heat removal for portable electronics, large scale systems and power electronics used for transportation.

Materials and Methods

The object of the study is the system in Figure 2. This system starts with a heat generating object to be cooled. The object has an attached heat spreader that covers one full face. The thermoelectric module is attached to the face of the heat spreader. On the opposite face of the heat spreader is the cooled object. There is a thermal grease in between the module and the heat spreader and between the heat spreader and cooled object. The faces of the heat spreader and cooled object that are not covered by the thermoelectric module are covered by thermal insulation. The perimeter of the cooled object is not insulated; it is exposed to the ambient air temperature. The face area of the cooled object that is attached to the heat spreader is much larger than the area of the edges of the cooled object. The heat generating object is approximately the size of an automotive pouch type battery cell. The detailed dimensions are in Table I.

SPICE model.—There are two main SPICE models that make up the system model used for the investigation herein. In terms of physical components, the first model is that of the thermoelements in the cooling module. The second part of the system model consists of the copper interconnects connecting the thermoelements, solder joints between the copper and thermoelements, alumunia dielectric plates, thermal grease between the alumina plates and heat spreader, thermal grease between the heat spreader and cooled object, heat spreader, heat generating object and thermal insulation. The distinction between the two models is given because they were created during two separate developments. The model for all of the physical components with exception of the thermoelements will be discussed in detail herein. The thermoelement model will be discussed briefly.

The key features of the 1D thermoelement model are distributed mass and distributed Joule heat generation within the thermoelements. This allows the model to accurately predict transient pulse cooling temperatures and heat flows. The details of the thermoelement model

Table I. System Model Properties; Excluding Thermoelement Properties.

	Component	Dimension [mm]	Number of Nodes	Thermal Conductivity [W/m K]	Density [kg/m^3]	Specific Heat [J/kg K]
Cold Side	Al Heat Spreader	165 × 230 × 1	25	204[72]	2700[72]	900[72]
	Mass	165 × 230 × 9	125	32[73]	2323[73]	1605[73]
	Alumina Dielectric	0.70	6	230[72]	3260[74]	740[74]
	Cu Interconnects	0.3000	6	386[72]	8960[72]	385[72]
	Tin/lead Solder Joint	0.0500	6	48[72]	not modeled	not modeled
	Thermal Grease	0.0235	6	3.7[75]	not modeled	not modeled
Hot Side			constant temperature			
Both Sides	Polyurethane Foam Insulation	165 × 230 × 25.4	25	0.35[76]	39[77]	1450[78]

Redistribution subject to ECS terms of use (see ecsdl.org/site/terms_use) unless CC License in place (see abstract).

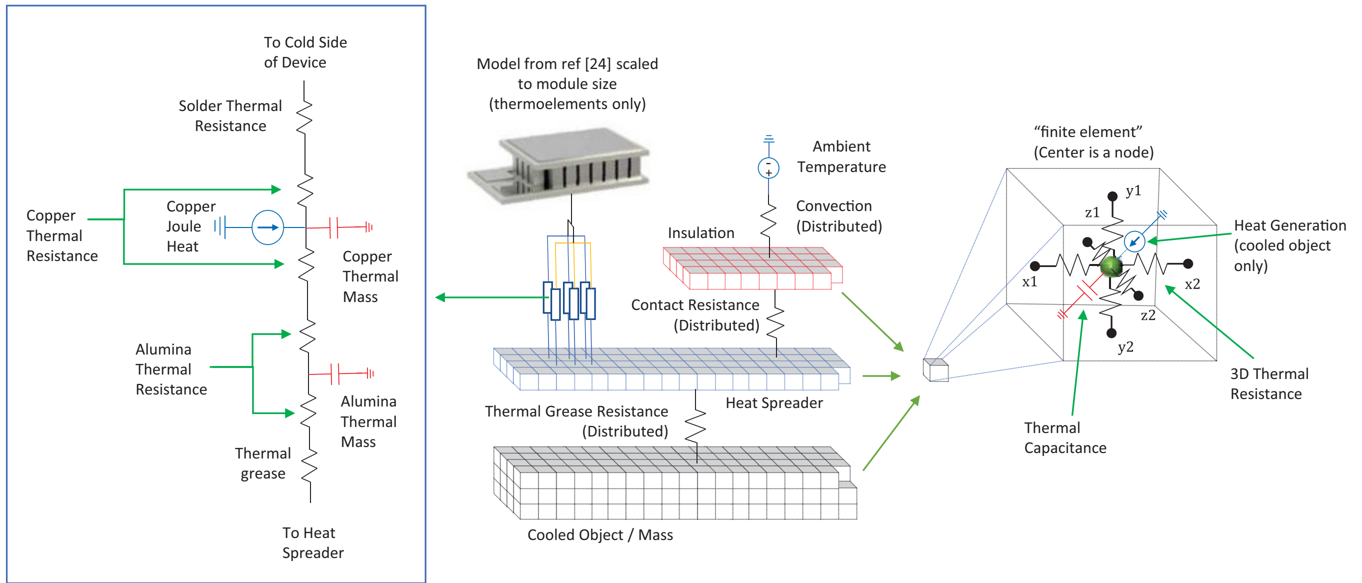

Figure 3. SPICE Model.

and its validation against experimental data can be found in previous work.[24,49]

The system model consists of networked electrical components whose values are specified using electrical-thermal analogies. These electrical circuits are numerically solved simultaneously for transient responses using SPICE software.

With exception of the thermoelement model, the schematic in Figure 3 details the networked electrical components used for the system model. The heat generating object, the heat spreader and the insulation all use a 3D arrangement of grouped electrical components with a node in the center to model the physics. These groupings of electrical components are analogous to "finite elements". Resistors are used in the x, y and z direction to capture three-dimensional thermal resistance and temperature gradients within the physical components. This 3D arrangement was modified from Sullivan et al.[65]

The model of the cooled object consists of 125 nodes. There are five nodes in the X dimension, 5 nodes in the Y dimension and 5 in the Z dimension. The resistors can be modeled with anisotropic properties however for the work herein they are isotropic. The thermal resistance value for each resistor in K/W is calculated by Equation 11.

$$R_{thX} = \left(\frac{L_x}{k_x A_{yz}}\right)\left(\frac{N_p}{R_{count}}\right) \quad [11]$$

Equation 11 is an example of the calculation for the x-direction heat flow. Here, $L_x/k_x A_{yx}$ is the total thermal resistance in the x-direction of the 3D cooled object. Here L_x is the length of the cooled object in the x-direction. k_x is the thermal conductivity of the cooled object in the x-direction. A_{yz} is the area normal to heat flow in the x direction. This is the area made up of the y and z dimensions of the cooled object. This portion of the equation could stand alone if the cooled object was modeled with one large resistor. The cooled object however is modeled with multiple parallel strings of resistors for which heat flows in the x-direction. For this reason, this total resistance must be multiplied by the number of parallel strings of resistors that run in the x-direction of the cooled object and terminate on the yz-plane (N_p). This gives the total resistance of each parallel string. Once this is found, it must be divided by the number of resistors in one of the strings (R_{count}). This process is repeated for the y and z direction thermal resistance.

Multiplying the total thermal resistance by the number of parallel strings may sound counter intuitive. This is analogous to using ten smaller pipes to flow water rather than one large pipe. Each pipe has a resistance to flow that is ten times higher than the one pipe yet there are ten pipes in parallel so the same water flows.

A capacitor is connected to the center node of each 3D grouping to model the transient nature of heat transfer within a mass. The thermal capacitance was evenly distributed between all nodes. The thermal capacitance at each node is the product of the total volume V, density ρ and specific heat capacity C_p divided by the number of nodes N as shown in Equation 12. The density, specific heat capacity and dimensions to calculate volume can be found in Table I.

$$C_{PerNode} = \frac{V\rho C_p}{N} \quad [12]$$

For the heat generating object, the heat generation was modeled at each node with a current source and this distributed the total heat generation evenly throughout the distributed mass. Potential exists to model this heat generation non-uniformly if desired.

In between the heat spreader and cooled object there is thermal grease. The thermal grease thermal interface resistance was modeled using distributed resistors. There is one resistor connecting each node of the heat spreader to each node at the top surface of the cooled object. Six resistors were used to model the thermal grease between the alumina and heat spreader. One resistor also connected each node between the between the insulation and the heat spreader to model thermal contact resistance. Only one resistor is shown in the schematic of Figure 3 for clarity. Every node of the insulation was connected to every node of the heat spreader with exception of the six nodes that were connected to the module. Insulation was modeled as depicted in Figure 2. That is with insulation surrounding the module and on both side of the cooled object.

For the thermal grease, to determine the value of the thermal interface resistances, the values in Table II are multiplied by the total area of the face for which the thermal grease interfaces. This gives the thermal interface resistance in K/W. The total thermal resistance is not only this interface resistance but is the thermal resistance of the grease layer itself combined with an interface resistance on both sides of the grease layer as shown in Equation 13. These three resistances were calculated for an entire physical part area and then totaled up. This total was then multiplied by the number of parallel resistors that connected between all of the nodes. This gives the thermal resistance at each resistor in the model as shown in Equation 14. It was assumed that the interfaces resistance was the same on either side of the grease layer. In reality the interface resistance on both sides would differ due to different surface characteristics on either side of the thermal grease.

Redistribution subject to ECS terms of use (see ecsdl.org/site/terms_use) unless CC License in place (see abstract).

Table II. Thermal Interface Resistance [m^2K/W].

Cold Side: Alumina - Thermal Grease	6.3×10^{-6}[75]
Cold Side: Thermal Grease - Spreader	6.3×10^{-6}[75]
Cold Side: Spreader - Thermal Grease	6.3×10^{-6}[75]
Cold Side: Thermal Grease - Mass	6.3×10^{-6}[75]
Mass - Insulation	8×10^{-2}[79]
Hot Side: Heat Exchanger	Constant Temperature (no interface resistance)

$$Rth_{Total} = Rth_{grease} + Rint_{grease} + Rint_{grease} \quad [13]$$

$$R_{resistor} = Rth_{Total} N \quad [14]$$

The ambient temperature was modeled using distributed voltage sources at each node of all physical parts exposed to the ambient. Constant temperature at these voltage sources was used however, the model is capable of using a time varying ambient temperature. Natural convection at each finite element was modeled using a resistor. Equation 15 is used to capture this thermal resistance. This model also has the capability to use adiabatic or radiative boundary conditions.

$$R_{convection} = \frac{1}{hA} \quad [15]$$

In Equation 15, A is the area exposed to ambient air and h is the convective heat transfer coefficient. Like the thermal resistance calculation above, the total resistance must be multiplied by the number of nodes on the surface exposed to the ambient.

For the convective heat transfer coefficients modeled herein, a simplified method of finding convection heat transfer coefficients was used.[70,71] Different heat transfer coefficients were used depending on if the surfaces exposed to ambient were vertical, horizontal facing up or horizontal facing down.

In between the thermoelements and the heat spreader, the thermal resistances of the solder, copper and alumina were modeled with series resistors in six parallel strings. This can be seen on the left side of Figure 3. Joule heat generated within the copper is captured in the model using a current source. The Joule heat was calculated using I^2R where I is the electrical current in the thermoelectric modules and R is the electrical resistance of the copper interconnects on the cold side of the device. This total heat generation was divided by six and then applied to each of the six current sources.

The total thermal capacitance for each component can be calculated per Equation 12. Before inputting the thermal capacitance variable, the total capacitance must be divided by the number of nodes in the physical part. This allows the model to capture the distributed mass transient heat transfer. The density, specific heat capacity and dimensions to calculate volume can be found in Table I.

The mass and Joule heat of the solder were not included due to the small magnitude of each. Depending on the accuracy needed, future model improvements may include these items. Additional future items may include the thermal interface resistance between the thermoelement and solder, the solder and copper and between the alumina and copper.

For the thermoelement module model, no optimizing was done in regard to the size and number of couples. The number of couples was simply scaled in order to satisfy a steady state cooled object temperature of 35°C. at its specified internal heat generation. Since the heat generating object was chosen as the size representing a battery cell, 35°C was chosen because it is a common thermal management target temperature for lithium ion battery cells.

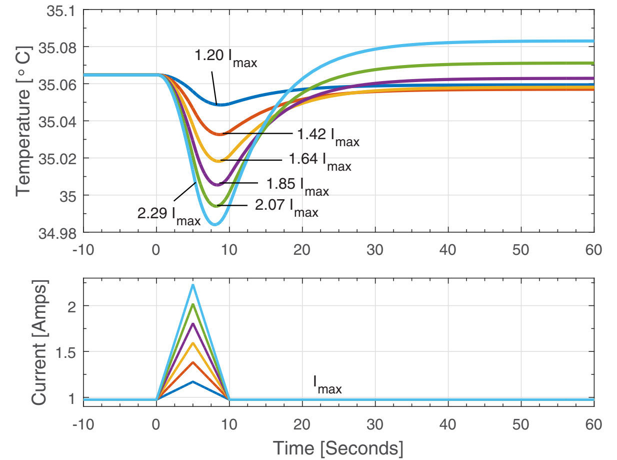

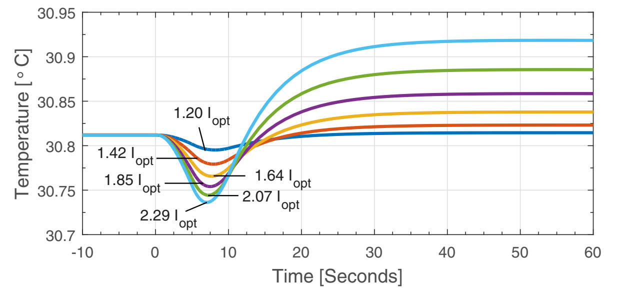

Figure 4. Effect of Pulse-Height on Average Cooled Object Temperature (a) Starting Pulses from I_{max} (b) Starting Pulses from I_{opt}.

Pulse-Height, I_P/I_{max}

Figure 4 shows the effect of pulse-height on average cooled object temperature for pulses starting from both I_{max} and I_{opt} steady current. It is seen that some of the pulses provided a net heat removal compared with steady operation as shown by the lasting temperature reduction for pulses starting from I_{max}. All pulses starting from I_{opt} provide a net heating effect over steady state operation that can be seen from the lasting increased average temperature of the cooled object. This temperature increase eventually reduces back to the steady state value with additional time beyond that shown in the figure. The increase in temperature is due to the transient penalty being larger than the transient advantage and creating a net heat addition. Some current pulses provide a net cooling because the transient advantage is larger than the transient penalty. For a better understanding of transient advantage and transient penalty, next the cooling rate $\dot{Q}_c$ will be investigated.

Figure 5 shows the effect of the pulse-height on $\dot{Q}_c$ vs. time. The upward spike in $\dot{Q}_c$ is due to the instant interfacial Peltier cooling at T_c (transient advantage). The downward spike is due to the time delayed volumetric Joule heat (transient penalty). For pulses starting from I_{max} the upward spike is larger than the downward spike. This is not the case for pulses starting from I_{opt}. For pulses starting from I_{opt}, this leads to higher object temperature due to a net heat input from the pulse.

Power consumption, ($\dot{W}_n$) is approximated by the steady state Equation 4. Each of the terms of the equation, however, are time delayed from one another for transient operation. Electrical current happens instantly. The temperatures of T_h and T_c take time to change. This and the fact that power is the square of current creates a non-linear shape of the power pulse.

Figure 6 shows the effect of various pulse-heights on COP. COP decreases during all pulses. COP is defined by Equation 5. The drop in COP is due to time constant separation between $\dot{Q}_c$ and $\dot{W}_n$.

Redistribution subject to ECS terms of use (see ecsdl.org/site/terms_use) unless CC License in place (see abstract).

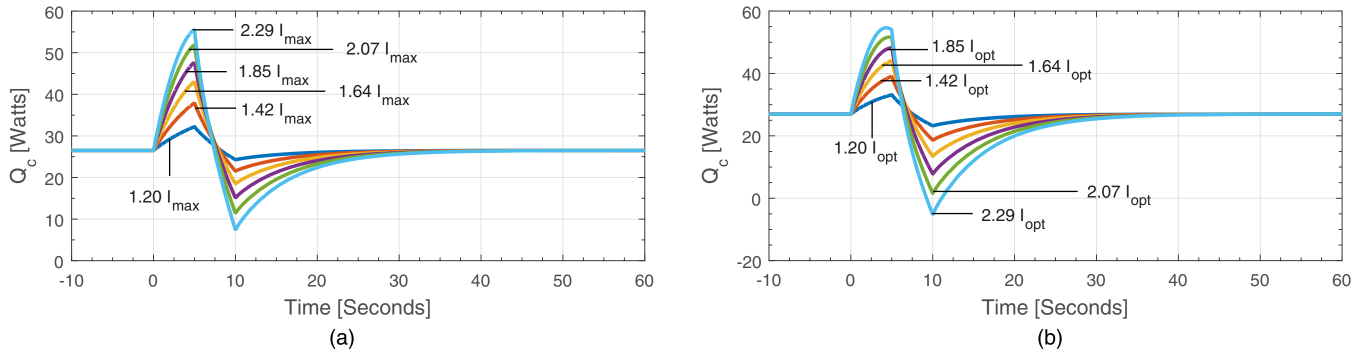

Figure 5. Effect of Pulse-Height on $\dot{Q}_c$ (a) Starting Pulses from $I_{\max}$ (b)Starting Pulses from I_{opt}.

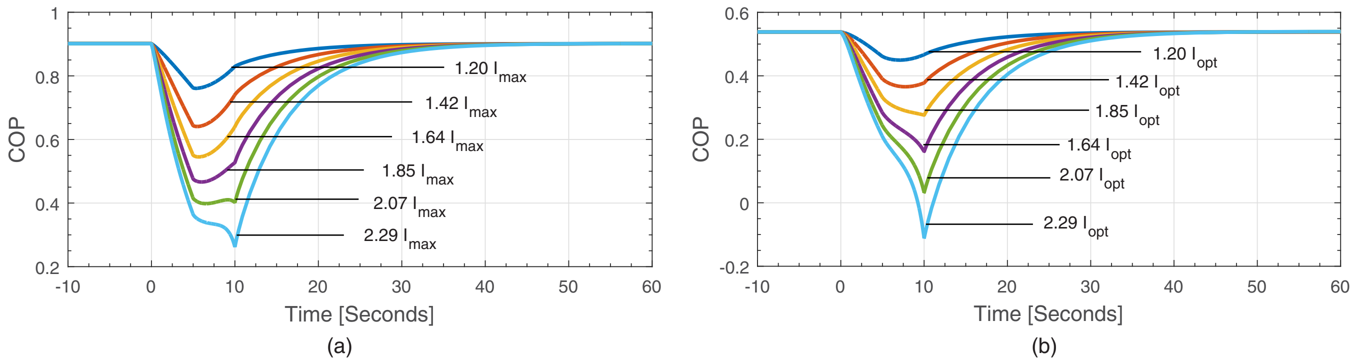

Figure 6. Effect of Pulse-Height, $I_P/I_{\max}$ on COP (a) Starting Pulses from $I_{\max}$ (b) Starting Pulses from I_{opt}.

The current and for the most part power in the equation for COP happens instantly. The $\dot{Q}_c$ is time delayed. For COP this means a fast increase in $\dot{W}_n$ before $\dot{Q}_c$ can react proportionally. Additionally, power input is a function of current squared, so as the current increases during the pulse, power input increases exponentially. $T_h - T_c$ increases during the pulse which further drives up power input from the Seebeck effect. These effects can be seen by the definition of power input from Equation 4.

Pulse Duration

Figure 7 shows the effect of leaving the same magnitude current pulse on for an increasing amount of time. For the current pulse starting from $I_{\max}$, average cooled object temperature during and after the pulse is lower than that of steady state. This suggests a net heat removal from the object during the pulse event.

For the current pulses starting from I_{opt}, (not shown) average cooled object temperature becomes lower with longer pulse duration however the average object temperature recovers to a temperature higher than it otherwise would have been in the absence of a pulse. This suggests the heat removal with a current pulse starting from I_{opt} has a lower net Q_c than steady state operation.

If the current pulses are left on longer or for a infinite time period, the thermoelectric device would simply be operating at a new steady state current. Operating the device at a steady state current higher than $I_{\max}$ will provide a higher $\dot{Q}_c$, however, operating at a current higher than I_{opt} will not due to the higher proportion of Joule heat relative to Peltier cooling at those current levels.

Figure 8 shows a trend of COP decreasing with each successive increase in pulse duration. This happens for the current pulses starting from I_{opt} (not shown) and $I_{\max}$. This happens because the time spent at higher current levels on average is longer for the longer pulse durations. At higher currents Joule heating increases and is parasitic to Peltier cooling so there is less $\dot{Q}_c$ relative to the power input. This combined with the faster time constant of power consumption drive COP down.

Interface Resistance Between Heat Spreader and Device

Figure 9 compares the effect on $\dot{Q}_c$ of linearly changing thermal interface resistance for the cold side of the device. Looking at steady state, the highest Q_c is for the lowest thermal interface resistance as expected. This changes for transient operation between 5 and 10 seconds. During this time, the highest $\dot{Q}_c$ is seen for the highest thermal interface resistance.

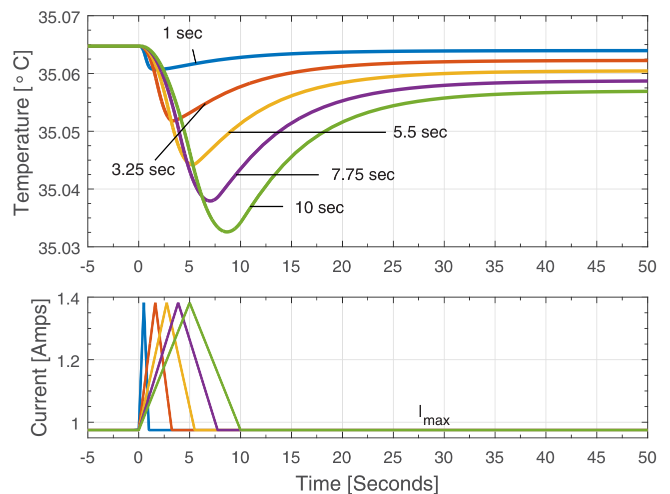

Figure 7. Effect of Pulse Duration on Cooled Object Temperature.

Redistribution subject to ECS terms of use (see ecsdl.org/site/terms_use) unless CC License in place (see abstract).

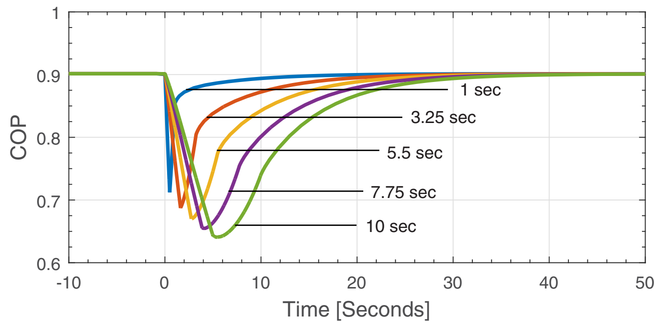

Figure 8. Effect of Pulse Duration on COP.

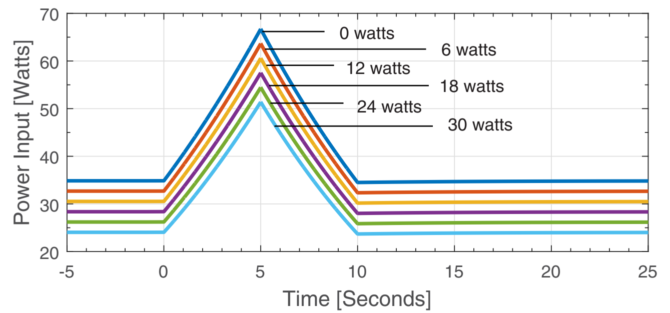

Figure 11. Effect of Cooled Object Heat Generation on $\dot{W}_n$.

Because of the higher thermal interface resistance, between 5 and 10 seconds, instead of the T_c junction pulling heat from the heat generating object, it pulls more heat from the thermoelement. When the thermoelement is cooled, it creates a reservoir for time delayed Joule heat to fill. This prevents some of the time delayed Joule heat from reaching T_c. This in turn increases $\dot{Q}_c$ for the same input current and raises the COP in Figure 10. Looking at Figure 10, at about 6 seconds, the highest thermal interface resistance started heading toward the highest COP. It is known from the analysis of Figure 9, that $\dot{Q}_c$ for the highest thermal interface resistance went from lowest during steady state and increasing current to the highest $\dot{Q}_c$ during the decreasing current portion of the pulse and for a time there after. This effect can be seen in Figure 10.

The same effects on $\dot{Q}_c$ and COP that were seen with changes in interface resistance between the cold side of the device and the heat spreader where also seen with changes in interface resistance between the heat spreader and the cooled object.

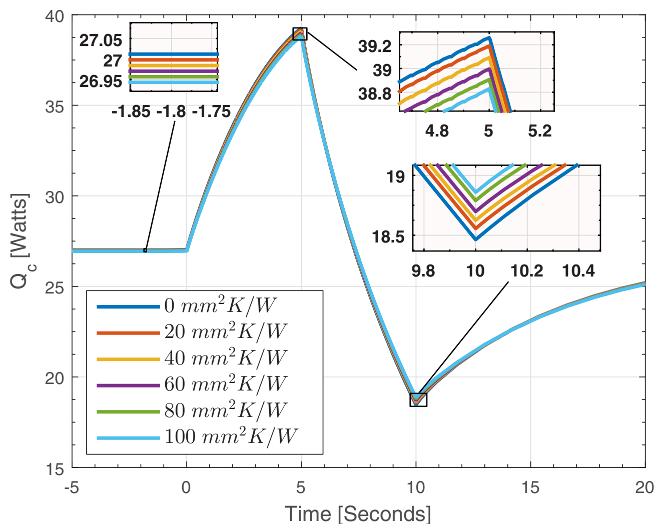

Figure 9. Effect of Changing Device Cold Side Interface Resistance on Q_c.

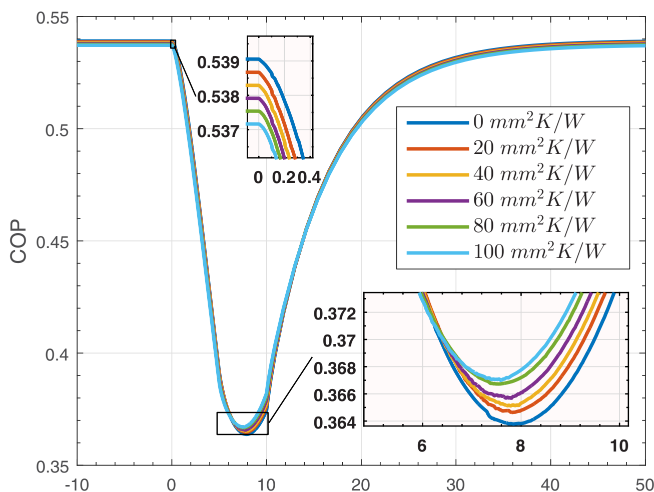

Figure 10. Effect of Changing Device Cold Side Interface Resistance on COP.

Internal Heat Generation in the Cooled Object

Figure 11 shows the effect of increased heat generation in the cooled object and its effect on $\dot{W}_n$. The highest cooled object heat generation rates are the highest T_c temperature and reduce power consumption to the lowest levels. Equation 4 shows increasing T_c, and keeping T_h constant reduces the power consumption of the device. When T_c is higher than T_h, the Seebeck effect lowers power consumption. When T_c is the same as T_h, the net Seebeck effect is zero so it does not change power consumption. When T_c is lower than T_h the Seebeck effect increases power consumption.

Under the modeled scenario, 18 to 30 watts of internal heat generation in the cooled object represents a negative ΔT across the thermoelement. That is, $T_c > T_h$. A positive ΔT, $T_h > T_c$ is observed for 0 to 12 watts. At approximately 15 watts, the ΔT is zero. The effect of the pulse on COP is much greater when starting from a negative ΔT than it is for a positive ΔT.

The $\dot{Q}_c$ rate of change is very similar between all heat generation rates. This makes the main driver for a reduction in COP for all of the plotted curves to be $\dot{W}_n$.

For some of the positive ΔT runs in Figure 12, there is an observable increase in COP for the first 0.5 to 1 second of the pulse. This is due to $\dot{Q}_c$ and $\dot{W}_n$ relative to each other in time from Equation 5. The smaller $\dot{W}_n$ rate for the zero-watt internal heat generation plot takes longer to increase at a greater rate than $\dot{Q}_c$ relative to the other heat generation runs. However, after about 1 second, the exponentially increasing $\dot{W}_n$ rate dominates Equation 5 leading to reduced COP for the remainder of the pulse.

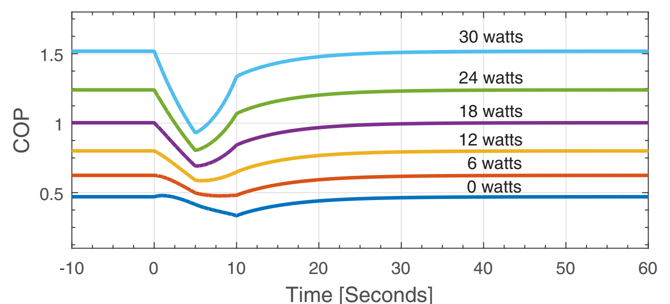

Figure 12. Effect of Cooled Object Heat Generation on COP.

Redistribution subject to ECS terms of use (see ecsdl.org/site/terms_use) unless CC License in place (see abstract).

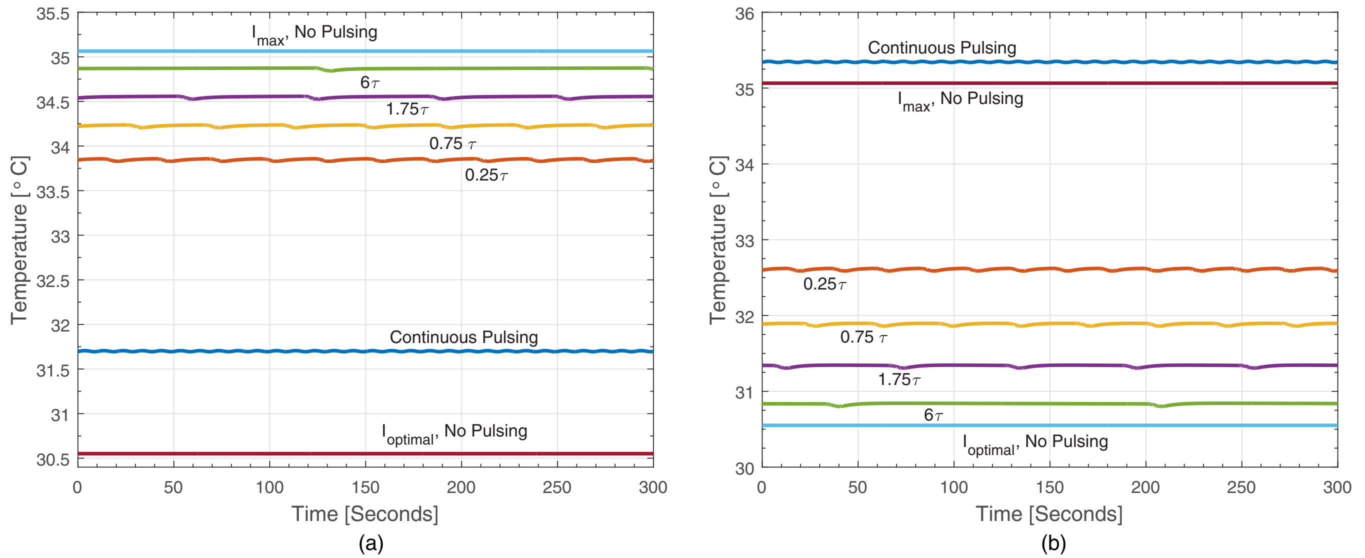

Figure 13. Effect of Time Between Pulses on Cooled Object Temperature (a) Pulses Starting from $I_{\max}$ (b) Pulses Starting from I_{opt}.

In pulse-height studies, minimum COP driven by time delayed Joule heat and time constant differences between $\dot{Q}_c$ and $\dot{W}_n$. Minimum COP was seen at 10 seconds. With variable object heat generation, Seebeck driven COP reductions reached a minimum at around 5 seconds for the higher internal heat generation rates. For the lower heat generation rates, the lowering of COP is initially dominated by the Seebeck effect but later by time delayed Joule heat.

Consecutive Pulsing

Figure 13 shows the effect of various times between current pulses and its effect on average cooled object temperature. Here, the model was allowed to run to quasi-steady state before recording the data. The time between pulses used is the time constant (Equation 10) for temperature to decay back to steady state after peak temperature during the transient penalty in Figure 1.

For pulses starting from $I_{\max}$, the heat generating object temperature is colder than steady state $I_{\max}$ and coldest for continuous pulses with the least steady state spacing. The temperature of the heat generating object never gets as cold as the I_{opt} steady state current. For the plot with current pulses starting from I_{opt}, I_{opt} steady current provides the lowest heat generating object temperature. The largest space between pulses provides the greatest amount of cooling which is opposite of what is seen with pulses starting with $I_{\max}$.

It is known that I_{opt} is the current that provides maximum cooling at steady-state. If current pulses start from I_{opt}, the average current will be higher than I_{opt} which will reduce the cooling. If more pulses are added to the same time span, the average current will be higher and provide a further decrease in cooling. This reduction in cooling is due to exponentially higher Joule heat at higher currents but only a linear amount of Peltier cooling added with higher current.

The current pulse-height and duration for the pulses starting from $I_{\max}$ was chosen to have an average current greater than $I_{\max}$ but less than I_{opt}. Therefore, additional cooling is seen with increased pulse frequency with pulses starting from $I_{\max}$. The most cooling that could be achieved with pulses starting from $I_{\max}$ is when the average current of the pulses over time is equal to I_{opt}.

If the average current is found for one pulse and one steady state rest period before the next pulse, the average of the two will be the average current for an infinite number of pulses. This is also the case for $\dot{Q}_c$ and COP. If it is known from one COP transient and one COP steady period that the average COP is lower than the steady state COP, no number of added pulses will improve the COP. From this and the above information, it is seen that using a correctly designed current pulse starting from $I_{\max}$ with an average current at or below I_{opt} can be used to increase cooling. However, the pulsed cooling will have a lower COP than steady state when its average current is equal to the steady state current.

Figure 14 is provided to show the relationship between current, power consumption, $\dot{Q}_c$ and COP during continuous pulses. Here pulses start from $I_{\max}$. From steady state $\dot{Q}_c$, an increase in $\dot{Q}_c$ is seen with the pulse followed by a decrease. The increase is larger than the decrease which leads to net cooling. No matter an increase or decrease in $\dot{Q}_c$, the COP is always reduced during the pulse. Here we can conclude that continuous pulses increase cooling but lower COP when everything is time averaged.

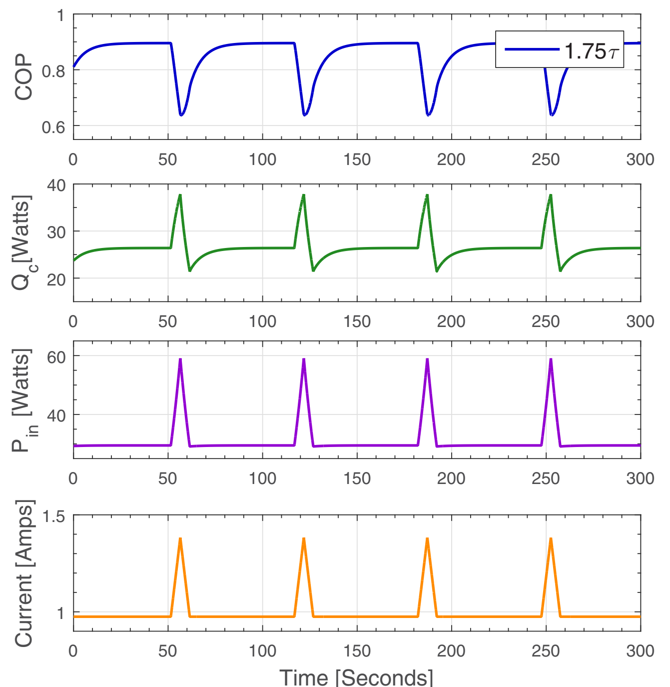

Figure 14. Repeating Pulses - 1.75τ Spacing. Relationship between Current, Power Input, $\dot{Q}_c$ and COP.

Redistribution subject to ECS terms of use (see ecsdl.org/site/terms_use) unless CC License in place (see abstract).

Conclusions

Pulsed current Peltier cooling has applications where short bursts of increased cooling are required for a short time. Examples are pulsed laser sensors and on-chip hot spot cooling.

A few pulsed current studies[67,55,68] have shown increases in cooling rate and/or COP over steady-state operation utilizing either single or consecutive current pulses. These studies however did not show transient results for COP, power consumption, or $\dot{Q}_c$ relative to a steady-state baseline. Furthermore there was no explanation why benefits were seen with pulse cooling compared to steady-state. It was the objective herein to show the transient data and provide an explanation of cooling and COP behavior.

To study pulse cooling herein, a thermoelectric cooling system for a heat generating object was simulated with a detailed SPICE model using electrical-thermal analogies and solved for transient responses. This work examined the effects of pulse cooling with isosceles current pulses on transient $\dot{Q}_c$, COP, power consumption and average cooled object temperature. $I_{\max}$ and I_{opt} steady-state pulse starting currents where used for comparison of cooling rates and COP. Variable operating conditions and system variables including pulse-height, pulse duration, cooled object heat generation rates, interface resistance and a series of repeating current pulses where studied.

Coefficent of Performance (COP) Key Takeaways:

COP depends on the rates of $\dot{Q}_c$ and $\dot{W}_n$ relative to each other at any given time. In most cases COP during a current pulse was reduced but in some cases there was a small increase. The reasons for this are as follows.

1. The time constant of $\dot{W}_n$ is faster than $\dot{Q}_c$, this drives the denominator of the COP equation down before the numerator can react proportionally. As a result, COP decreases.
2. $\dot{Q}_c$ increases in the shape of an upside down parabola as a function of increasing current, however $\dot{W}_n$ always increases as a function of the square of current in the absence of Seebeck induced voltage. This drives COP down and drives it down at a faster rate at increased currents.
3. During a pulse, time delayed Joule heat reaches T_c. This reduces $\dot{Q}_c$ relative to $\dot{W}_n$ and drives COP down.
4. Decreased T_c and increased T_h during the pulse increases the Seebeck voltage which increases $\dot{W}_n$ relative to $\dot{Q}_c$ and contributes to a lower COP.

Some situations resulted in a small transient COP increase.

1. Higher thermal interface resistances produce a higher COP than lower interface materials for part of the pulse transient. This is opposite of conventional steady state thinking. With higher thermal interface resistance, during a current pulse, the path to heat flow from T_c to the thermoelement becomes more favorable than the path to the cooled object. When this happens, early on in the pulse, the cold end of the thermoelement is cooled, thus creating a reservoir for time delayed Joule heat. For a short time, this prevents some Joule heat from reaching T_c. $\dot{Q}_c$ is therefore increased relative to power consumption and COP increases.
2. A small COP increase was seen with zero heat generation within the cooled object. During the pulse, the rate of $\dot{Q}_c$ briefly outpaced $\dot{W}_n$. Shortly thereafter, increased $\dot{W}_n$ dominated the direction of COP downward. It is possible in this case, a small thermal reservoir was created in the thermoelements which reduced the amount of Joule heat reaching T_c for a short time.

Cooling Rate, ($\dot{Q}_c$) Consecutive Pulses, Key Takeaways:

1. Using repeating consecutive pulses can be accomplished in two ways. One way is to start the second pulse after steady-state is achieved following the first pulse. Another way of utilizing consecutive pulses is to start the second pulse before steady-state has been achieved after the first pulse.
2. It was found that consecutive pulses starting from I_{max} with a steady-state period in between pulses can be utilized to increase cooling over time periods longer than one transient advantage. The average current during the pulsing needs to be less than I_{opt} for this to occur. However the downside of using current pulses to achieve this increased cooling is that COP is decreased. This happens because operating at the higher currents leads to higher Joule heat generation relative to Peltier cooling.
3. It was found that consecutive pulses starting from I_{opt} cannot be utilized to increase cooling longer than one transient advantage period. Here the initial higher $\dot{Q}_c$ is followed by a larger magnitude decrease in $\dot{Q}_c$ which averages out to a lower net $\dot{Q}_c$ during repeating consecutive pulses.
4. Starting a new current pulse prior to completion of the transient penalty of the first pulse leads to lower $\dot{Q}_c$ due to Joule heat accumulation in the thermoelement. This leads to lower COP and a higher temperature at T_c even with a constant temperature boundary condition at T_h.
5. Any application that utilizes current pulses starting from I_{max} or I_{opt} will have a lower average COP than operating at a steady-state current equal to the average current during consecutive pulsing. The reason is that operation during pulses generates at larger percentage of Joule heat relative to the Peltier cooling even though Peltier cooling is also increased at higher currents. This happens because Joule heat is the square of current and Peltier cooling is a linear function of current.

Analysis of pulsed Peltier cooling is useful to gain a deep understanding of both transient and steady-state thermoelectric cooler operation. Future research may focus on further detailed analysis of low or no heat generation pulsed cooling with low pulse heights where small increases in COP were found during the work herein.

References

1. iNEMI, Thermal Management TWG, Technical Report, iNEMI, 2017.
2. L. Technologies, *Thermoelectric handbook*, 2014.
3. E. Karampasis, N. Papanikolaou, D. Voglitsis, M. Loupis, A. Psarras, A. Boubaris, D. Baros, and G. Dimitrakopoulos, Active thermoelectric cooling solutions for airspace applications: the thermicool project, *IEEE Acess*, (2017).
4. Thermoelectricsolutions.com, 9 advantages of solid-state thermoelectric thermal management technology, 2017.
5. D. Enescu and F. Spertino, Applications of hybrid photovoltaic modules with thermoelectric cooling, *Energy Procedia*, **111**, 904 (2017).
6. R. Enright, S. Lei, G. Cunningham, I. Mathews, R. Frizzell, and A. Shenb, Integrated thermoelectric cooling for silicon photonics, *ECS Journal of Solid State Science and Technology*, **6**, N3103 (2017).
7. J. Skovajsa, M. Kolcek, and M. Zlek, Phase change material based accumulation panels in combination with renewable energy sources and thermoelectric cooling, *Energies*, **10** (2017).
8. Design of an Atmospheric Water Generator: Harvesting Water Out of Thin Air, 2016.
9. H. Al-Madhhachi and G. Min, Effective use of thermal energy at both hot and cold side of thermoelectric module for developing efficient thermoelectric water distillation system, *Energy Conversion and Management*, **133**, 14 (2017).
10. A. Attar and H. Lee, Designing and testing the optimum design of automotive air-to-air thermoelectric air conditioner (teac) system, *Energy Conversion and Management*, **112**, 328 (2016).
11. Improving efficiency of a vehicle HVAC system with comfort modeling, zonal design, and thermoelectric devices, Deer Conference, 2012.
12. R. Yang, G. Chen, G. J. Ravi Kumar, A. Snyder, and J.-P. Fleurial, Transient cooling of thermoelectric coolers and its applications for microdevices, *Energy Conversion and Management* (2005).
13. T. Barnhart, A. J. Piggott, D. Kossakovski, and K. Smith, Distributed battery thermal management using thermoelectrics, 2014. SAE Thermal Management Symposium.
14. A. J. Piggott, D. Kossakovski, and T. Barnhart, Thermoelectric based thermal management system, 2015.
15. A. J. Piggott, D. S. Thomas, and D. C. Guerithault, Graphite thermoelectric and/or resistive thermal management systems and methods, 2016.
16. D. Kossakovski, A. J. Piggott, and T. Barnhart, Battery thermal management with themoelectrics, 2016.
17. D. Kossakovski and A. J. Piggott, Thermoelectric-based thermal management of electrical devices, 2015.
18. J. Yang and F. R. Stabler, Automotive applications of thermoelectric materials, *Journal of Electronic Materials*, **39** (2009).
19. G. J. Snyder, M. Soto, R. Alley, D. Koester, and B. Conner, Hot spot cooling using embedded thermoelectric coolers, in: 22nd IEEE SEMI-THERM Symposium, 2006.
20. TECA, Thermoelectric air conditioner applications, 2015.

Redistribution subject to ECS terms of use (see **ecsdl.org/site/terms_use**) unless CC License in place (see abstract).

21. T. Makansi, M. J. Berman, S. Wood, J. L. Franklin, and M. N. Evers, Distributed thermoelectric string and insulating panel and applications for local heating, local cooling, and power generation from heat, 2012.
22. S. B. Riffat and X. Ma, Improving the coefficient of performance of thermoelectric cooling systems: a review, *International Journal Of Energy Research*, **28**, 753 (2004).
23. L. Trachtenberg and P. W. Trachtenberg, Vehicle thermoelectric cooling and heating food and drink appliance, 1989.
24. A. J. Piggott and J. S. Allen, Peltier supercooling with isosceles current pulses: A response surface perspective, *ESC Journal of Solid-State Science and Technology*, **6**, N3045 (2017).
25. L. Stilbans and N. Fedorovich, Cooling of thermoelectric cells under nonstationary conditions, *Soviet Physics. Technical Physics*, **3**, 460 (1958).
26. J. Parrott, The interpretation of the stationary and transient behavior of refrigerating thermocouples, *Solid-state electronics*, **1**, 135 (1960).
27. K. L. Findlay, Study of fast transient behavious of peltier junctions, *Soild-State Electronics*, **3**, 239 (1961).
28. R. R. Heikes and R. W. Ure, *Thermoelectricity: science and engineering*, Interscience Publishers New York, 1961.
29. M. Idnurm and K. Landecker, Experiments with peltier junctions pulsed with high transient currents, *Journal of Applied Physics*, **34**, 1806 (1963).
30. B. VP, Enhancement of thermoelectric cooling in non stationary operation, *Soviet Physics*, **14**, 293 (1969).
31. K. Landecker, Some further remarks on the improvement of peltier junctions for thermoelectric cooling, *Energy Conversion*, **14**, 21 (1974).
32. G. E. Hoyos, K. Rao, and D. Jerger, Fast transient response of novel peltier junctions, *Energy Conversion*, **17**, 45 (1977).
33. R. Field and H. Blum, Fast transient behavior of thermoelectric coolers with high current pulse and finite cold junction, *Energy conversion*, **19**, 159 (1979).
34. A. R. Kumar, R. Yang, G. Chen, and J. Fleurial, Transient thermoelectric cooling of thin film devices, *Materials Research Society Symosia Proceedings*, **626**, Z11 (2000).
35. Geometric Effects on the Transient Cooling of Thermoelectric Coolers, volume 691, Boston, Massachusetts, U.S.A., 2001.
36. G. J. Snyder, J.-P. Fleurial, T. Caillat, R. Yang, and G. Chen, Supercooling of peltier cooler using a current pulse, *Journal of Applied Physics*, **92**, 1564 (2002).
37. T. Thonhauser, G. D. Mahan, L. Zikatanov, and J. Roe, Improved supercooling in transient thermoelectrics, *Applied Physics Letters*, **85**, 3247 (2004).
38. D. Mitrani, J. Salazar, A. Turi, M. J. Garcia, and J. A. Chavez, Transient distributed parameter electrical analogous model of te devices, *Microelectronics Journal*, **40**, 1406 (2009).
39. O. Sullivan, M. P. Gupta, S. Mukhopadhyay, and S. Kumar, Thermoelectric coolers for thermal gradient management on chip, in: ASME 2010 International Mechanical Engineering Congress and Exposition, *American Society of Mechanical Engineers*, 187 (2010).
40. J. Mao, H. Chen, H. Jia, and X. Qian, The transient behavior of peltier junctions pulsed with supercooling, *Journal of Applied Physics*, **112**, 014514 (2012).
41. O. A. Sullivan, Embedded Thermoelectric Devices For On-chip Cooling And Power Generation, Ph.D. thesis, Georgia Institute of Technology, 2012.
42. L. M. Shen, F. Xiao, H. X. Chen, and S. W. Wang, Numerical and experimental analysis of transient supercooling effect of voltage pulse on thermoelectric element, *International Journal of Refrigeration*, **35**, 1156 (2012).
43. M. Redmond, K. Manickaraj, O. Sullivan, S. Mukhopadhyay, and S. Kumar, Hotspot cooling in stacked chips using thermoelectric coolers, Components, Packaging and Manufacturing Technology, *IEEE Transactions on*, **3**, 759 (2013).
44. M. Manno and W. Peng, A. Bar-Cohen, Pulsed thermoelectric cooling for improved suppression of a germanium hotspot, Components, Packaging and Manufacturing Technology, *IEEE Transactions on*, **4**, 602 (2014).
45. M. Ma, A numerical study on the temperature overshoot characteristic of a realistic thermoelectric module under a current pulse operation, *International journal of heat and mass transfer*, **72**, 234 (2014).
46. L. Shen, The step-change cooling performance of miniature thermoelectric module for pulse laser, *Energy conversion and management*, **80**, 39 (2014).
47. H. Lv, X.-D. Wang, T.-H. Wang, and J.-H. Meng, Optimal pulse current shape for transient supercooling of thermoelectric cooler, *Energy*, **83**, 788 (2015).
48. M. V. Manno, On-chip Thermoelectric Hotspot Cooling, Ph.D. thesis, University of Maryland, 2015.
49. A. J. Piggott, Transient Thermoelectric Supercooling: Isosceles Current Pulses From a Response Surface Perspective And The Performance Effects Of Pulse Cooling a Heat Generating Mass, Master's thesis, Michigan Technological University, 2015.
50. M. Ma, J. Yu, and J. Chen, An investigation on thermoelectric coolers operated with continuous current pulses, *Energy Conversion and Management*, **98**, 275 (2015).
51. M. Ma and J. Yu, Experimental study on transient cooling characteristics of a realistic thermoelectric module under a current pulse operation, *Energy Conversion and Management*, **126**, 210 (2016).
52. H. Lv, X.-D. Wang, and C.-H. Wang, Tian-Huand Cheng, Improvement of transient supercooling of thermoelectric coolers through variable semiconductor cross-section, *Applied Energy*, **164**, 501 (2016).
53. H. Lv, X.-D. Wang, J.-H. Meng, T.-H. Wang, and W.-M. Yan, Enhancement of maximum temperature drop across thermoelectric cooler through two-stage design and transient supercooling effect, *Applied Energy*, **175**, 285 (2016).
54. S. Lin, M. Maa, J. Wangb, and J. Yu, Experiment investigation of a two-stage thermoelectricexperiment investigation of a two-stage thermoelectric cooler under current pulse operation, *Applied Energy*, **180**, 628 (2016).
55. S. Manikandan, S. Kaushik, and R. Yang, Modified pulse operation of thermoelectric coolers for building cooling applications, *Modified pulse operation of thermoelectric coolers for building cooling applications*, **140**, 145 (2017).
56. L. Chen and J. Lee, Effect of pulsed heat power on the thermal and electrical performances of a thermoelectric generator, *Applied Energy*, **138** (2015).
57. L. Chen and J. Lee, Efficiency enhancement of an industrial-scale thermoelectric generator system by periodically inputting thermal power, *Energy Conversion and Management*, **75** (2016).
58. R. McCarty and K. P. Hallinan, Enhancing thermoelectric energy recovery via modulations of source temperature for cyclical heat loadings, *Journal of Heat Transfer*, **129**, 749 (2007).
59. Y. Yana and J. Malen, Periodic heating amplifies the efficiency of thermoelectric energy conversion, *Energy & Environmental Science*, **6**, 1267 (2013).
60. W.-H. Chen, P.-H. Wua, X.-D. Wangb, and Y.-L. L. c, Power output and efficiency of a thermoelectric generator under temperature control, *Energy Conversion and Management*, **127**, 404 (2016).
61. T. 8th International Symposium on Advanced Topics In Electrical Engineering (Ed.), Pulsed Operation Analysis of the Thermoelectric Generators Used in Space Applications, 2013.
62. H. Lee, The thomson effect and the ideal equation on thermoelectric coolers, *Energy*, **56**, 61 (2013).
63. H. Lee, A. M. Attar, and S. L. Weera, Performance prediction of commercial thermoelectric cooler modules using the effective material properties, *Journal of Electronic Materials*, **44**, 2157 (2015).
64. S. Lineykin and S. Ben-Yaakov, Analysis of thermoelectric coolers by a spice-compatible equivalent-circuit model, *IEEE Power Electronics* (2005).
65. O. Sullivan, B. Alexandrov, S. Mukhopadhyay, and S. Kumar, 3d compact model of packaged thermoelectric coolers, *Journal of Electronic Packaging*, **135**, 031006 (2013).
66. Spice Compatible Equivalent Circuit of the Energy Conversion Process in Thermoelectric Modules, 2004.
67. A. Miner, A. Majumdar, and U. Ghoshal, Thermoelectromechanical refrigeration based on transient thermoelectric effects, *Applied physics letters*, **75**, 1176 (1999).
68. S. Garimell, T. Harirchian, A. Kraus, K. Geisler, A. Bar-Cohen, B. Yang, P. Wang, M. Arik, A. Setlur, S. W. Jr, J. J. Shiang, and G. L. Solbrekken, Encyclopedia of Thermal Packaging, volume 1-6, World Scientific, 2013.
69. J. A. Balderas-Lopez, Measurements of thermal effusivity of liquids using a conventional photoacoustic cell, *Review of Scientific Instruments*, **70**, (1990).
70. W. McAdams, *Heat Transmission*, 3rd ed., McGraw-Hill, 1954.
71. F. Incropera and D. DeWitt, *Fundamentals of Heat and Mass Transfer*, John Wiley & Sons, 1985.
72. Melcor, Thermoelectric handbook, Unknown.
73. S. Drakea, D. Wetz, J. Ostanek, S. Miller, J. Heinzel, and A. Jain, Measurement of anisotropic thermophysical properties of cylindrical li-ion cells, *Journal of Power Sources*, **252**, 298 (2014).
74. Accuratus.com, Aluminum nitride, ain ceramic properties, 2013.
75. Thermal Interface Materials for Power Electronics Applications, 2008.
76. M. Wang and N. Pan, Modeling and prediction of the effective thermal conductivity of random open-cell porous foams, *International Journal of Heat and Mass Transfer*, **51**, 1325 (2008).
77. W. Witkiewicz and A. Zielinski, Properties of the polyurethane (pu) light foams, *Advances in Materials Science*, **6**, 36 (2006).
78. F. of European Rigid Polyurethane Foam Associations, Thermal insulation materials made of rigid polyurethane foam (pur/pir) properties - manufacture, 2006.
79. Thermopedia.com, Thermal contact resistance, Website, 2011.

Redistribution subject to ECS terms of use (see **ecsdl.org/site/terms_use**) unless CC License in place (see abstract).